VELOCITY-RESOLVED OBSERVATIONS OF Hα EMISSION FROM COMET C/1995 O1 (HALE-BOPP)

Jeffrey P. Morgenthaler (jpmorgen@alum.mit.edu) and Walter M. Harris
University of Wisconsin–Madison, Space Astronomy Laboratory, 1150 University Ave., Madison, WI 53706, USA

Frank Scherb
University of Wisconsin–Madison, Department of Physics, 1150 University Ave., Madison, WI 53706

Nathaniel E. Doane
University of Wisconsin–Madison, Department of Astronomy, 1150 University Ave., Madison, WI 53706

Ronald J. Oliversen
NASA/Goddard Space Flight Center, Code 681, Greenbelt, MD 20771, USA

Abstract. We present hydrogen Balmer-α spectra of comet C/1995 O1 (Hale-Bopp) recorded on 5 nights from 1997 February 1 to April 19 by a high-resolution ($\Delta v = 5\ \mathrm{km\ s^{-1}}$) Fabry-Pérot spectrometer for a $4'.1$ ($\sim\ 2.7 \times 10^5$ km) FOV centered $5'$ sunward of the nucleus. The Hα line profile is an important diagnostic of photolytic heating in cometary atmospheres. Extraction of the spectra from the Fabry-Pérot ring images was complicated by obscuration of the telescope FOV due to Hale-Bopp's low elevation, but the measured H-α line widths of 11–13 $\mathrm{km\ s^{-1}}$ (FWHM) are insensitive to the spectral extraction technique. The line widths are consistent with estimates derived from a successful model of Hale-Bopp's hydrogen Lyman-α coma assuming the inner coma is opaque to Hα. We discuss methods for improving the spectral extraction technique and deriving a precise instrument profile which will allow the detailed shape of the line profile to constrain coma models.

Keywords: Comets, C/1995 O1 (Hale-Bopp), Fabry-Pérot spectrometers, hydrogen Balmer$-\alpha$ coma, line widths, photolytic heating

1. Introduction

When a comet approaches within a few AU of the sun, sublimation of icy volatiles, particularly H_2O, CO, and CO_2 create an atmosphere which is free to expand into interplanetary space. At the extreme base of the atmosphere, the excess energy of sublimation and collisions between the sublimation products determine the velocity distribution of the expanding atmosphere. Where the atmosphere becomes transparent to solar UV radiation, cometary molecular species begin to photodissociate. At this point, the atmosphere is still dense enough for frequent ballistic collisions to occur, so the excess energy of photodissociation becomes the driver of bulk outflow

acceleration. The dominant cometary volatile, H_2O, and its daughter, OH, have excess energies of photodissociation ranging from a few to several tens of eV (Huebner et al., 1992). Conservation of momentum necessitates that most of this energy is transferred to the hydrogen atom. Thus, it is ballistic collisions with these hot hydrogen atoms that determines the majority of cometary atmosphere outflow velocity structure.

Cometary outflow velocity can be determined in several ways, for example: *in situ* measurements, extraction of Doppler information from emission line profiles, the Greenstein effect, and measurement of radial surface brightness variation of a particular coma line. This last technique requires accurate knowledge of the lifetime against photodestruction of the emitting species and, if the field of view (FOV) of the observation is not large enough, previous knowledge of the production rate of the comet in that species (Cochran and Schleicher, 1993).

Extraction of Doppler information from emission line profiles is the most common method for determining comet atmosphere bulk outflow velocities (e.g., Bockelée-Morvan et al., 1990). Since typical outflow velocities are $\sim 1\ \mathrm{km\ s^{-1}}$, the high sensitivity and spectral resolving power in the radio make it the natural spectral range for these measurements. In cometary comæ, only molecular transitions are available in the radio, so direct observation of the hot hydrogen atoms that drive the outflow must be done at shorter wavelengths.

Excited by solar Lyman-β radiation, hydrogen Balmer-α (Hα) is the brightest line available to ground-based observers for spectroscopic determination of the cometary hydrogen velocity distribution. A collaboration from the University of Wisconsin–Madison and NASA Goddard Space Flight Center recorded high-resolution Hα spectra on five nights during the perihelion passage of comet C/1995 O1 (Hale-Bopp). The measured line widths of $11 - 13\ \mathrm{km\ s^{-1}}$ (FWHM), are significantly larger than the intrinsic velocity dispersion of $4.5\ \mathrm{km\ s^{-1}}$ predicted by a successful model of the Lyα coma (Combi et al., 2000). Radiative transfer calculations based on this model suggest that the inner regions of the comet atmosphere are opaque to Hα, resulting in a loss of photons from the line center and a corresponding increase in the line width (Combi, 2002, private communication). Preliminary calculations suggest a good match between the measured and modeled line widths, but further work on both fronts is necessary in order to extract all the information these data have to offer on the driving mechanism of cometary atmosphere outflow.

2. Observations

The Hα observations presented here were part of a comprehensive observing campaign of comet Hale-Bopp conducted by the University of Wisconsin–

Madison and NASA Goddard Space Flight Center (Morgenthaler et al., 2001; Harris et al., 2002; Glinski et al., 2001; Anderson, 1999, Harris et al., these proceedings, Morgenthaler et al., these proceedings). A 50 mm dual-etalon pressure-tuned Fabry-Pérot (FP) spectrometer coupled to a CCD detector (Roesler, 1974; Coakley and Roesler, 1994) located at the north port of the main McMath-Pierce Solar telescope on Kitt Peak recorded high-resolution spectra in [C I] 9850 Å, [O I] 6300 Å, and Hα. The instrument configuration and the [C I] 9850 Å results are presented by Oliversen et al. (2002). The instrument field-of-view (FOV) is derived by Morgenthaler et al. (2001, Figure 5) and has an effective diameter of $4'.1$.

Hα spectra of the comet were recorded on 7 nights, 5 of which were usable (Table I). The intended observing procedure was to record one or two spectra with the telescope FOV centered on the nucleus and the rest centered $5'$ sunward. As expected, the nucleus-centered spectra were dominated by the H_2O^+ line that is coincident with Hα. The sunward observations showed no evidence of this emission. On two nights, sunward observations could not be taken. Because of the limited FOV of the telescope guider, we estimate that the FOV drifted $30'' \sim 60''$ during the sunward observations (Oliversen et al., 2002).

As this pressure-tuned dual-etalon FP was used as part of a multiwavelength campaign, the gas pressure in the chambers was changed by ~ 0.5 atmospheres every night. This induced a slight bowing of the pressure chambers in which the individual etalons were mounted. The two glass plates of each etalon remained highly parallel (a necessary condition to proper FP functioning), but the orientation of the etalons with respect to each other would change slightly, which induces second-order effects. The chambers (since replaced) were originally part of a pressure-scanned system in which the FP bullseye was imaged onto a photomultiplier. This configuration was not very sensitive to misalignment because the individual bullseyes cover a large range in angle space. By imaging the FP ring pattern onto a CCD, many spectral elements can be sampled simultaneously, greatly increasing instrument sensitivity and observing efficiency (Coakley and Roesler, 1994). However the FP rings become narrower with increasing radius (decreasing wavelength), which translates into an increase in sensitivity to the relative alignment of the etalons. The effect of misalignment is to decrease the intensity of the primary transmission peak of the system since the output of the first etalon is no longer efficiently coupled to the input of the second. This in turn increases the width of the instrument response and decreases the contrast between the primary transmission peak and the higher order peaks (ghosts). The last effect complicates the fitting of spectral lines whose relative spacing happen to fall near intervals of the higher-resolution etalon free-spectral-range ($\sim 50\ \mathrm{km\ s^{-1}}$ for these observations).

We have developed a physically realistic model of the dual-etalon FP system that accounts for all these effects. An interface between this model and the `curvefit` routine of IDL is being written that will allow us to use our extensive set of post-campaign calibration data to determine the invariant parameters of the FP system, such as the etalon spacings and reflectivities. Next we will fitted the model to the nightly calibration data to determine a reasonable starting point for the parameters likely to vary through the night, such as the relative orientation of the etalons, their relative wavelength tune, and the FP ring pattern center. For each comet FP ring image, we will repeat the planned spectral extraction and fitting procedures detailed in §3 for a grid of these parameters. Using the geocoronal Hα line present in each cometary spectrum and accurate measurements and predictions of its line shape and intensity (Nossal et al., 1997, 1998; Bishop et al., 2001), we will find the best-fit values for these parameters. This technique will also be applied to our [O I] 6300 Å and [C I] 9850 Å data, likely resulting in a significant decrease in the scatter seen in the intensity values of these data (Morgenthaler et al., 2001; Oliversen et al., 2002).

3. Reduction

We have completed preliminary reduction of the Hale-Bopp Hα data set using the software developed for the [C I] analysis of Oliversen et al. (2002). Figure 1 shows a sample FP ring image of Hale-Bopp Hα emission processed by standard bias subtraction, flat-fielding and cosmic-ray removal algorithms. The various telescope obscuration effects described by Oliversen et al. are indicated. The noticeable left-right gradient in the image is not understood at this time: it is seen in most of the Hale-Bopp Hα data but not in the [O I] or [C I] comet images or any of the calibration data. Since the Hα observations were generally taken at less favorable viewing geometries than the [C I] and [O I] observations, this may be an exaggerated effect of white light scattering from the telescope superstructure: scattering of atmospheric emission lines into the telescope beam was noted in the other observations. In an attempt to avoid these effects, we selected small areas of each image, such as that indicated in Figure 1, from which to extract the FP spectra (e.g., Figure 2). The vertical lines at each point of Figure 2 are the error bars derived from the number of CCD electrons in each spectral bin. We experimented with extracting spectra from different portions of the ring image and found that the Hα linewidth was insensitive to the region used but the continuum level and shape, as well as the area under the Hα line were quite sensitive to the selected region.

In order to make the grid search of FP parameters discussed in §2 practical, we are designing a program that will automatically extract the best spectrum

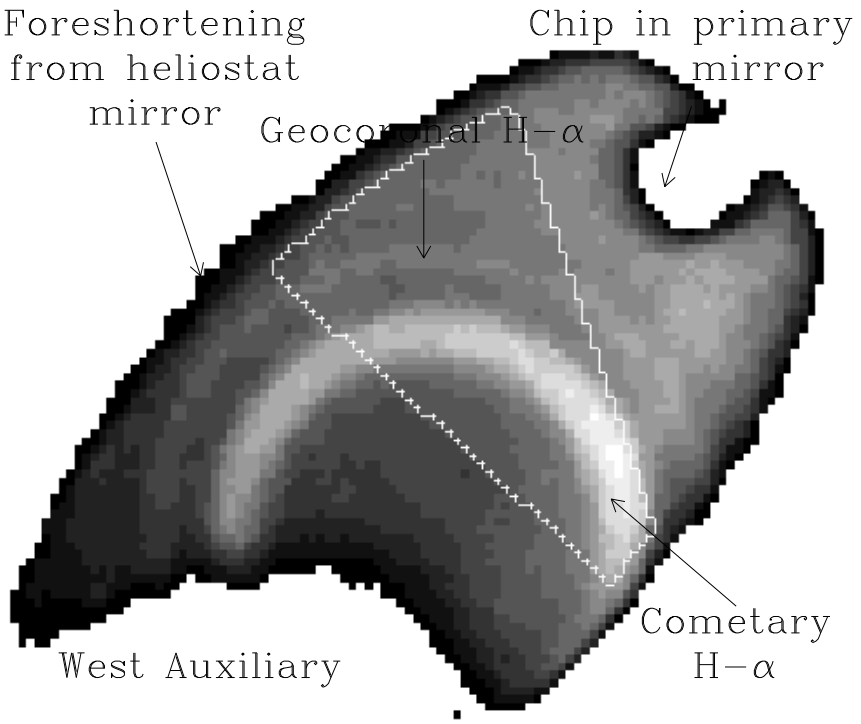

Figure 1. Fabry-Pérot (FP) ring image of Hale-Bopp in Hα recorded UT 1997 April 16 03:18. The primary (#2) mirror was imaged directly onto the CCD detector and was conjugate with the FP ring pattern. The #2 mirror was not illuminated uniformly, hence the incomplete rings. The gradient across the image is likely from scattered light and affects the continuum shape but not the comet or geocoronal line widths. The outline shows the section of the image used to make the spectrum in Figure 2.

from each image assuming a particular orientation of the etalons. The first step in the program will be to extract spectra from small pie-slices arranged azimuthally about the assumed FP ring pattern center. The small statistical error bars in Figure 2 indicate that many azimuthal bins can to be used. Since each spectral bin should be invariant as a function of angle or, if there is etalon misalignment, vary in a prescribed way, data beyond the edges of the usable image, and any severe problems from gradients, can be easily removed. The remaining data will then be fitted by the assumed azimuthal variation of the ring, resulting in a best-fit value and uncertainty for each spectral bin.

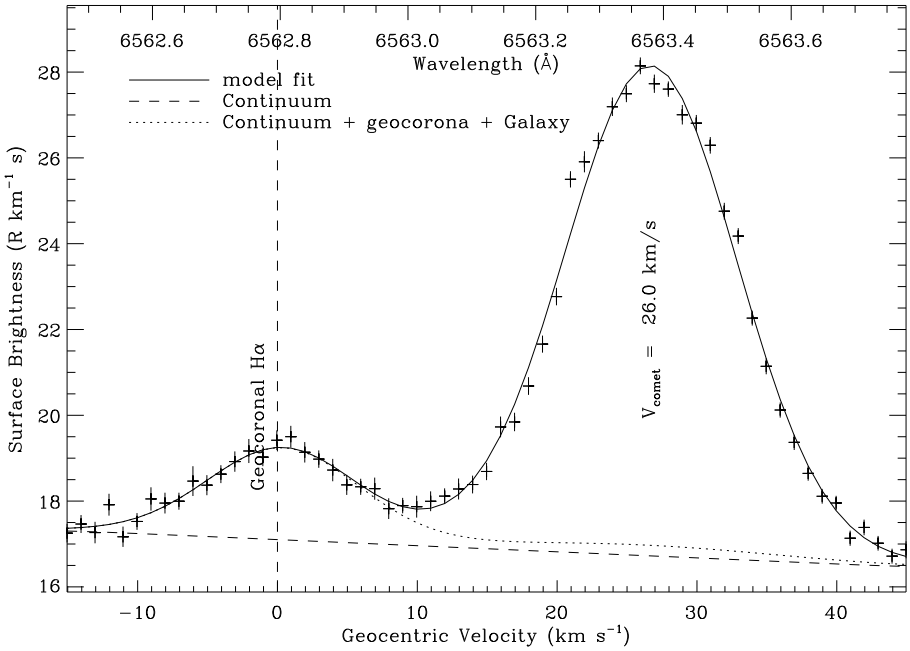

Figure 2. Fabry-Pérot (FP) spectrum, with statistical error bars, of the portion of the ring image shown in Figure 1. The spectrum was fitted using the instrument response shown in Figure 3 and a model composed of two variable Gaussians, a sloping continuum and two fixed Gaussians representing the Galaxy.

We plan to use the model of the FP instrument response discussed in §2 for our future spectral analysis. For the purposes of this work we approximated the instrument response with a Voigt profile fit to the Ce 6300.21 Å line of our post-campaign calibration data. The line had to be fit in order to remove the ghost of the Ce 6295.58 Å line. The resulting instrument profile, shown in Figure 3, has a width of 4.2 $\mathrm{km\ s^{-1}}$ (FWHM). We checked this result by fitting the airglow [O I] 6300 Å line recorded on 1997 April 14 (Morgenthaler et al., 2001, Figure 4, 4.7 $\mathrm{km\ s^{-1}}$) and the Th-Ar 6564.44 Å calibration line recorded on 1997 March 6 (4.8 $\mathrm{km\ s^{-1}}$). Although the airglow line may just be resolved by this instrument, variation in the orientation of the etalons is the most likely cause of the variations in these widths.

We used the instrument response shown in Figure 3 to fit Voigt profiles to the geocoronal and cometary emissions (solid line in Figure 2). Galactic emission determined from the Wisconsin Hα Mapper (WHAM) survey data (Reynolds, 1997, http://www.astro.wisc.edu/wham) and shown as the dotted line in Figure 2, was included as a fixed part of the continuum in the fits. The Gaussian line widths from these fits are given in Table I. The Lorentzian components of the comet fits always converged to small values; for the geocorona, they often had to be set to zero.

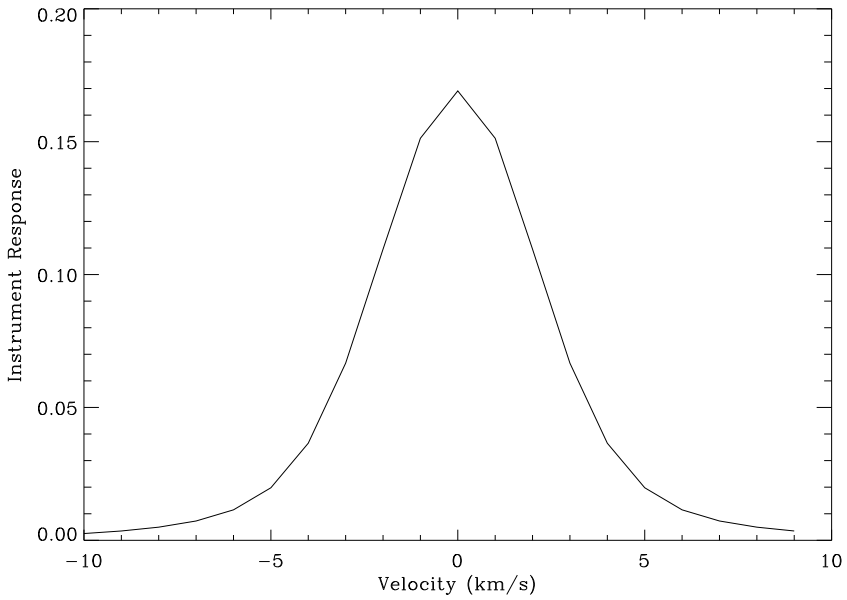

Figure 3. Estimate of the spectral response of the 50 mm FP spectrometer at Hα.

Preliminary results from the detailed FP response modeling discussed in §2 suggest that the difficulty we had constraining the geocoronal Hα line widths was due to the proximity of this line to a ghost of the cometary Hα line. Using fits to the nightly hydrogen-deuterium calibration spectra, we see evidence for an increase of the instrument profile width to 8 $\mathrm{km\ s^{-1}}$ in February with a corresponding decrease in the instrument sensitivity. This corresponds to a change of 0.5 $\mathrm{km\ s^{-1}}$ in the cometary Hα line width. We expect to be able to model and completely remove these effects in the final analysis.

4. Results

In spite of the planned improvements in the Hα spectral extraction and instrument profile generation, we do not expect much change in the line width results, summarized in the "dv_c" column of Table I, since we found these values to vary by no more than 0.5 $\mathrm{km\ s^{-1}}$ due to any of the effects discussed above. Thus, Hale-Bopp's measured Hα line width is $11 - 13\ \mathrm{km\ s^{-1}}$ (FWHM) for a $\sim 2.7 \times 10^5$ km FOV centered $\sim 3.3 \times 10^5$ km sunward of the nucleus.

The Hα line profile of comet Halley, measured with a similar instrument, was successfully modeled using a sophisticated Monte-Carlo code that

Table I. Preliminary Hα Results

UT (1997)	R[1]	$\dot{R}$[2]	Δ[3]	$\dot{\Delta}$[4]	FOV[5]	dv_g[6]	dv_c[7]
Feb 15 12:03	1.2017	-18.75	1.7209	-33.09	3.01	5.0	14.4
Mar 5 12:28	1.0291	-13.85	1.4273	-21.89	2.57	8.1	13.6
Apr 14 02:31	0.9431	7.58	1.4970	24.95	2.70	6[8]	11.4
Apr 14 02:37	0.9431	7.58	1.4971	24.95	2.70	6.7	11.0
Apr 14 02:48	0.9431	7.58	1.4972	24.96	2.70	6[8]	10.5
Apr 15 03:39	0.9478	8.14	1.5122	25.57	2.72	9.8	13.9
Apr 16 02:48	0.9525	8.64	1.5264	26.10	2.75	6[8]	11.9
Apr 16 03:05	0.9525	8.65	1.5266	26.11	2.75	10.2	13.0
Apr 16 03:18	0.9526	8.65	1.5267	26.12	2.75	10.5	13.0

[1]Heliocentric distance in AU.
[2]Heliocentric velocity in km s^{-1}.
[3]Geocentric distance in AU.
[4]Geocentric velocity in km s^{-1}.
[5]Field-of-view diameter in units of 10^5 km.
[6]Geocoronal Hα line width (FWHM) in km s^{-1}.
[7]Cometary Hα line width (FWHM) in km s^{-1}.
[8]Not well constrained

traces the evolution of individual particles in the comet atmosphere (Combi and Smyth, 1988a; Smyth et al., 1993). This code, which has also successfully matched observations of the Lyα coma in comets 1P/1982 U1 (Halley; Combi and Smyth, 1988b), C/1996 B2 (Hyakutake; Richter et al., 2000), and Hale-Bopp (Combi et al., 2000) predicts an intrinsic hydrogen velocity dispersion of 4.5 $\mathrm{km\,s^{-1}}$ for our FOV (Combi, 2002, private communication). Scaling the radiative transfer calculations of Richter et al. (2000) to the conditions in Hale-Bopp at the position of our FOV suggests that the top half of the Hα line is lost due to the optical depth effects (Combi, 2002, private communication). This results in an effective line width of $10 - 12$ $\mathrm{km\,s^{-1}}$, which is consistent with our measurements.

We intend to continue our analysis of the Hale-Bopp Hα data using the techniques discussed in §3 to reduce the magnitude of the relative systematic errors between data points to the level of the statistical error bars shown in Figure 2 or better. With the techniques discussed in §2, we expect to derive the instrument profile to similar accuracy. The resulting line profiles will provide a powerful constraint to detailed models of cometary atmosphere dynamics and coma emissions.

Acknowledgements

We would like to thank F. Roesler, E. Mierkiewicz, and M. Combi for valuable discussions. This work has been supported under NSF grant AST-9615625, NASA grant NAG 5-7952, and NASA contract NASW-97020.

References

Anderson, C. M.: 1999, *Earth, Moon, Planets* **78**, 99.

Bishop, J., Harlander, J., Nossal, S., and Roesler, F. L.: 2001, *J. Atmos. Sol.-Terr. Phys.* **63**, 341–353.

Bockelée-Morvan, D., Crovisier, J., and Gerard, E.: 1990, *A&A* **238**, 382–400.

Coakley, M. M. and Roesler, F. L.: 1994, *Proceedings of SPIE* **2266**, 122–132.

Cochran, A. L. and Schleicher, D. G.: 1993, *Icarus* **105**, 235–253.

Combi, M. R., Reinard, A. A., Bertaux, J., Quemerais, E., and Mäkinen, T.: 2000, *Icarus* **144**, 191–202.

Combi, M. R. and Smyth, W. H.: 1988a, *ApJ* **327**, 1026–1043.

Combi, M. R. and Smyth, W. H.: 1988b, *ApJ* **327**, 1044–1059.

Glinski, R. J., Post, E. A., and Anderson, C. M.: 2001, *ApJ* **550**, 1131–1139.

Harris, W. M., Morgenthaler, J., Mierkiewicz, E., Scherb, F., Oliversen, R., and Nordsieck, K., ????, these proceedings.

Harris, W. M., Scherb, F., Mierkiewicz, E. J., Oliversen, R. J., and Morgenthaler, J. P.: 2002, *ApJ* **578**, 996–1008.

Huebner, W. F., Keady, J. J., and Lyon, S. P.: 1992, *Astrophys. Space Sci.* **195**, 1–294.

Morgenthaler, J. P., Harris, W. M., Scherb, F., Anderson, C. M., Oliversen, R. J., Doane, N. E., Combi, M. R., Marconi, M. L., and Smyth, W. H.: 2001, *ApJ* **563**, 451–461.

Morgenthaler, J. P., Harris, W. M., Scherb, F., Roelser, F. L., Anderson, C. M., Doane, N. E., and Oliversen, R. J., ????, these proceedings.

Nossal, S., Roesler, F. L., and Coakley, M. M.: 1998, *J. Geophys. Res.* **103**, 381–390.

Nossal, S., Roesler, F. L., Coakley, M. M., and Reynolds, R.: 1997, *J. Geophys. Res.* **102**, 14541–14554.

Oliversen, R. J., Doane, N. E., Scherb, F., Harris, W. M., and Morgenthaler, J. P.: 2002, *ApJ* **581**. in press.

Reynolds, R. J.: 1997, *Science* **277**, 1446–1447.

Richter, K., Combi, M. R., Keller, H. U., and Meier, R. R.: 2000, *ApJ* **531**, 599–611.

Roesler, F. L.: 1974, in N. P. Carleton (ed.), *Methods of Experimental Physics*, Vol. 12, part A, Academic Press, New York, pp. 531–569.

Smyth, W. H., Marconi, M. L., Scherb, F., and Roesler, F.: 1993, *ApJ* **413**, 756–763.